Green Chemistry

PAPER

View Article Online
View Journal | View Issue

Cite this: *Green Chem.*, 2025, **27**, 11971

The recovery of valuable metals from spent ternary lithium-ion batteries by repurposing the pyrolysis gas

Zhen Xiong,[a,b,c] Hairong Zhang, *[a,b,c] Can Wang,[a,b,c] Haijun Guo,[a,b,c] Mengkun Wang,[a,b,c] Hailong Li,[a,b,c] Xuefang Chen,[a,b,c] Lian Xiong[a,b,c] and Xinde Chen *[a,b,c]

Received 5th July 2025,
Accepted 2nd September 2025

DOI: 10.1039/d5gc03423j

rsc.li/greenchem

To establish a recycling process for spent lithium-ion batteries (LIBs) suitable for industrialization, minimizing energy consumption and simplifying the recycling process are critical. Herein, we propose a roasting reduction method to recover valuable metals from spent LIBs by repurposing the pyrolysis gas of the LIBs. The pyrolysis gas serves as a reducing agent, while the carbon-based materials in the LIBs (graphite, electrolytes, separators, and binders) act as a carbon resource during the roasting process. The results show that the spent $LiNi_{0.65}Co_{0.15}Mn_{0.2}O_2$ (LNCM) cell can be completely reduced to Li, Ni, Co, Mn, or their respective compounds using pyrolysis gas at 550 °C. Through a combined environmentally friendly process of water leaching and citric acid leaching, 91.62% of Li, 98.71% of Ni, 99.46% of Co, and 98.51% of Mn are recovered from the roasted products. These recovery efficiencies are higher than that of carbothermal reduction using carbon-based materials in an inert atmosphere. The synergistic effect between the reductive gases in the pyrolysis gas and the carbon resource is a key factor enabling the reduction process of LNCM at lower temperatures compared to conventional carbothermic reduction under an oxygen-free atmosphere. Therefore, the recycling method based on the *in situ* reduction-leaching of LIBs is environmentally friendly, economical, and has promising applications in industrial scale-up.

Green foundation

1. This study proposes a roasting reduction method for spent $LiNi_{0.65}Co_{0.15}Mn_{0.2}O_2$ battery using pyrolysis gas from the gasification reaction of organic materials (graphite, electrolytes, separators, binders). Subsequently, metals can be recovered *via* hydrometallurgical processes without a reducing agent.
2. The synergistic effect of carbon and reducing gases can significantly lower the decomposition temperature of $LiNi_{0.65}Co_{0.15}Mn_{0.2}O_2$. Through a combined environmentally friendly process of water leaching and citric acid leaching, 91.62% of Li, 98.71% of Ni, 99.46% of Co, and 98.51% of Mn are recovered from the roasting products.
3. In future research, the proposed pyrolysis tail gas utilization technology may provide a more energy-efficient and economically viable recycling method for the spent lithium-ion batteries.

1. Introduction

With the increasing prevalence of electric vehicles (EVs) and mobile electronic devices, such as smartphones, tablets, and laptop computers, which have become indispensable in daily life, lithium-ion batteries (LIBs) have gained widespread adoption globally due to their long lifespan, high energy efficiency, and superior power density.[1,2] It is projected that by 2030, there will be approximately 253 million EVs worldwide.[3] In 2024, China's total LIB production has surpassed 1 TWh. Typically, the service life of LIBs ranges from 3 to 8 years, depending on usage patterns, leading to a significant accumulation of spent or discarded LIBs.[3,4] The cathode materials of spent ternary lithium-ion batteries contain hazardous substances, including carcinogenic and mutagenic elements such as nickel and cobalt, as well as toxic electrolytes. Improper disposal of spent LIBs poses substantial risks to human health and the environment.[5,6] Furthermore, critical minerals like lithium, nickel, and cobalt are characterized by their relatively

[a]*School of Energy Science and Engineering, University of Science and Technology of China, Hefei 230026, PR China*
[b]*Guangzhou Institute of Energy Conversion, Chinese Academy of Sciences, No. 2 Nengyuan Road, Tianhe District, Guangzhou 510640, PR China.*
E-mail: zhanghr@ms.giec.ac.cn, cxd_cxd@hotmail.com; Fax: +862037213916; Tel: +862087020234, +862037213916
[c]*R&D Centre of Xuyi Attapulgite Energy and Environmental Materials, Xuyi 211700, PR China*

low abundance and high production costs.[7] Therefore, the recycling of ternary lithium battery waste, such as spent $LiNi_xCo_yMn_{1-x-y}O_2$ (LNCM), holds considerable economic value and strategic importance.

Traditionally, the recycling of LIB waste is primarily categorized into three methods: pyrometallurgy, hydrometallurgy, and bio-metallurgy. Pyrometallurgy is a well-established high-temperature treatment process for the recovery of metals from spent LIBs. In this process, the organic binder is removed from the electrode material, and the reduced valuable metals are subsequently recovered in the form of an alloy. Pyrometallurgy is extensively employed in large-scale recycling due to its short reaction time, straightforward operation, and high adaptability to raw materials.[8] It enables the effective recovery of valuable metals such as Ni and Co. However, most lithium remains in the smelting slag, leading to a relatively low overall lithium recovery rate. Moreover, pyrometallurgy is an energy-intensive process (reaction temperature >1500 °C), requiring significant equipment investment and producing toxic gases.[9,10] The bio-metallurgy method is regarded as one of the most promising technologies for spent LIB recycling from both environmental and economic perspectives.[11,12] Bio-metallurgy offers high recycling efficiency and excellent separation effects; however, its long operating time, complex processes, and stringent fermentation conditions hinder its industrial application. Hydrometallurgy involves dissolving the cathode material with acid to extract metal ions, followed by separating these ions using extraction, precipitation, or electrochemical methods.[13] Hydrometallurgy, including acid leaching[14,15] and reduced ammonium leaching,[16] has been widely adopted due to its low energy consumption and high metal yield. Traditional inorganic acid leaching has the disadvantages of high corrosiveness and serious environmental pollution. In contrast, organic acid leaching has received widespread attention due to its advantages of environmental protection and high selectivity. Citric acid, as a cheap and common organic acid containing three carboxylic acid groups with good complexing ability and environmental friendliness, has been widely used in metal leaching.[17,18] Previous studies usually added chemical reductants such as H_2O_2 during the acid leaching process to enhance leaching efficiency; however, the extensive use of reducing agents results in substantial wastewater discharge and gas emissions during the leaching process, causing secondary pollution.[2]

In light of the limitations of single-process pyrometallurgy or hydrometallurgy for LIB recycling, the combined pyrometallurgy-hydrometallurgy recycling process has garnered increasing attention due to its high recycling efficiency and reduced energy consumption.[19] In the pyrometallurgy stage, the LNCM compound is first converted into water-soluble lithium compounds (LiOH or Li_2CO_3) and transition metals or their compounds through reduction roasting at medium temperatures (500–800 °C) by reducing agents such as hydrogen,[20] biomass,[21,22] anode powder,[16,23] and others. The high-valence states of transition metals can be reduced to easily leachable low-valence states during reduction roasting.[20,24] Subsequently, the recovery of metals is achieved *via* hydrometallurgical processes. Specifically, lithium can be effectively recovered in the form of LiOH or Li_2CO_3 by water leaching, while transition metals, including nickel, cobalt, and manganese, are recovered through acid leaching or ammonia leaching (without reducing agent).[25,26] Xie *et al.* found that the lithium ions present in $LiCoO_2$ or $LiNi_xCo_yMn_zO_2$ can be transformed into water-soluble LiOH in a hydrogen atmosphere at 450 °C. Over 98% of the lithium in the reduction products was obtained through the water-leaching process (lithium concentrations were 23.6 and 23.9 g L^{-1}).[20] Ma *et al.*[16] conducted a reduction roasting of $LiNi_xCo_yMn_zO_2$ powder at 650 °C for 1 h using spent anode powder as a reductant. Subsequently, 82.2% of Li (in the form of Li_2CO_3, obtained *via* evaporation crystallization) was recovered from the roasting product by water immersion. Additionally, selective ammonia leaching ($NH_3{\cdot}H_2O$ + $(NH_4)_2SO_3$) achieved the recovery of 97.7% nickel and 99.1% cobalt. Zhou *et al.*[22] introduced a pyrolysis process within the medium-temperature range (600–800 °C) using sawdust as a reducing agent, achieving 99% lithium recovery efficiency in the form of Li_2CO_3 from retired LNCM batteries and $LiMn_2O_4$. Hasan *et al.*[27] utilized carbothermal reduction of $LiCoO_2$ and waste coffee powder at 600 °C to reduce $LiCoO_2$ into Li_2CO_3 and Co, and recover 89.23% of Li and 93.27% of Co by water leaching process. They found that the synergistic effect of carbon and reductive gases produced during the pyrolysis of biomass is a critical factor for the transformation of $LiCoO_2$ at lower temperatures.

Spent LIBs contain significant amounts of organic materials, such as the anode electrode (graphite-based carbon material), electrolytes, separators, binders, *etc*.[28,29] These substances can vaporize into pyrolysis gases containing CO_2, CO, and H_2 at high temperatures.[22,30] Lithium salts in the electrolyte, such as $LiPF_6$, can transform into LiF and PF_5 during the pyrolysis process. A significant portion of LiF remains in the pyrolysis slag, whereas most of the PF_5 reacts with H_2O to generate HF and H_3PO_4.[31,32] Additionally, the thermal degradation of organic binders (polyvinylidene fluoride, PVDF) can also lead to the formation of HF.[33] Therefore, to prevent environmental pollution caused by the HF and pyrolysis oil, pyrolysis gases are typically treated using an alkaline solution and an ice bath to remove fluorinated compounds and recover condensable compounds.[34,35] In addition to condensable products, a large quantity of non-condensable gases (pyrolysis gases) also has significant value, the reducing gases (CO and H_2) in the pyrolysis gases can facilitate the roasting reduction of cathode materials. Therefore, using the generated pyrolysis gas as a feedstock for the reduction-roasting process of LIBs could help reduce the cost of the pyrometallurgical process and promote the industrial-scale disposal and recovery of spent LIBs. However, most previous studies have focused on the thermal reduction of cathode materials, with only a few reports addressing the pyrolysis of LIBs. Moreover, separating cathode materials from LIBs typically involves multiple processes, such as dismantling, crushing, and binder removal, which increase recycling costs.[36]

To the best of our knowledge, there is no report on utilizing pyrolysis gas for the thermal treatment of LIBs. In this study, we investigated and evaluated the feasibility of using pyrolysis gas derived from the gasification reaction of organic materials in LIBs to enhance valuable metal recovery during the reduction-roasting process of spent LNCM batteries. The roasting products were characterized by X-ray diffraction (XRD), scanning electron microscopy (SEM), and X-ray photoelectron spectroscopy (XPS). In the acid leaching process, citric acid was used for acid leaching without added H_2O_2. Li was recovered from the roasted products through water leaching, and then Ni, Co, and Mn were recovered from the water-leaching residue *via* acid leaching, while the metals' leaching efficiency was determined using inductively coupled plasma-optical emission spectrometry (ICP-OES). Furthermore, the pyrolysis behaviors of cathode materials and LNCM cells under pyrolysis gas were compared using thermogravimetric analysis (TGA), and the synergistic effect between pyrolysis gas reduction and carbothermal reduction was also explored.

2. Experiment

2.1 Materials

The spent LNCM batteries from electric vehicles were provided by local EV manufacturers. The spent battery was discharging the residual electricity by soaking in a 5 wt% NaCl solution, and then the battery shell was stripped away. The LNCM cell, without disassembling and crushing, including electrodes, membrane, Cu foil, and Al foils, was used as raw material. The cathode foil was obtained through manual disassembly, and the chemical compositions of the cathode material contained in the cathode foil were analyzed using XRD (X'Pert PRO MPD, PANalytical V.B., Netherlands) and ICP-OES (OPTIMA 8000, PerkinElmer, USA). The results showed that the mass content of lithium was 6.58%, nickel 38.52%, cobalt 8.74%, and manganese 10.71%, which indicated that the cathode material is $LiNi_{0.65}Co_{0.15}Mn_{0.2}O_2$. Meanwhile, the cathode foil was directly utilized as the raw material for cathode pyrolysis without any additional treatment.

2.2 Thermal treatment experiment

The LNCM cell was first pyrolyzed in a tube furnace, and the pyrolysis gas was analyzed by gas chromatography (GC, Agilent 7890A, USA). Then, the pyrolysis behavior of LNCM was examined under simulated pyrolysis gas. The roasting products were first leached in water to recover lithium, and then the water-leaching residues were subjected to citric acid leaching to recycle transition metals. A schematic diagram of the pyrometallurgy-hydrometallurgy process for recycling spent LNCM is shown in Fig. 1.

The composition of the pyrolysis gas was determined as follows: a piece of spent LNCM cell (10.20 ± 0.20 g) was rolled into a cylindrical shape and then placed in a sealed tube furnace (Φ 3 cm × 70 cm). The tube furnace was first flushed with N_2 for 15 min to remove air and then heated to 550 °C for 6 h. The exhaust gas was passed through an ice-water solution to remove trace amounts of condensable compounds such as HF and pyrolysis oil, *etc.*, and non-condensable gas was collected in airbags. The composition of the non-condensable gas was as follows: 75.60% of CO_2, 14.53% of CO, and 9.88% of H_2.

Based on the composition of the pyrolysis gas, we formulated a mixture of gases as the atmosphere for the roasting process of LNCM. For a typical roasting process, a piece of LNCM cell (10.20 ± 0.20 g) was introduced into a sealed vertical tube furnace under a gas mixture atmosphere (75% CO_2, 15% CO, and 10% H_2). The sample was roasted for 0.5–6 h at different temperatures (350 °C –750 °C) with different gas flow rates (5 mL min^{-1}–150 mL min^{-1}), respectively.

The roasting product was crushed and passed through a 200-mesh sieve; the sieve residue (aluminum foil and copper foil) and electrode powder were obtained. The lithium salt was separated by water leaching under constant stirring at 25 °C

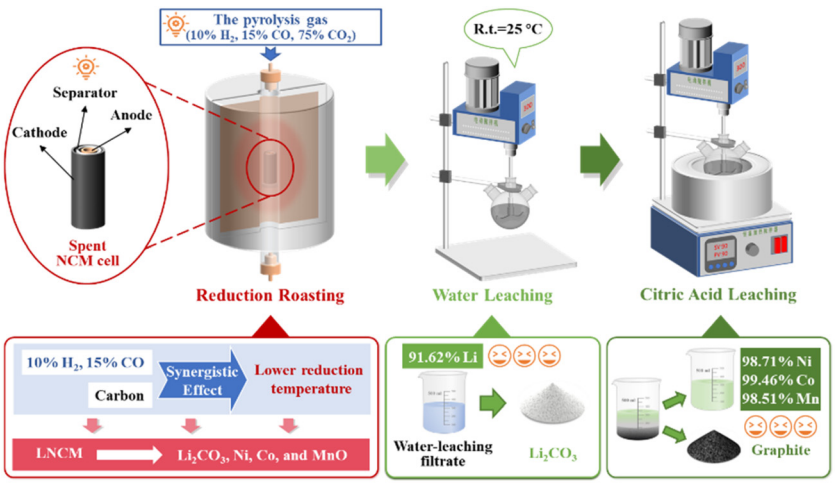

Fig. 1 Schematic diagram of the pyrometallurgy-hydrometallurgy process for recycling spent LNCM cell.

for 12 h. The ratio of deionized water to electrode powder was 50/1 (v/w). After water-leaching, the mixture was filtered, the Li_2CO_3 concentration in the filtrate was determined by ICP-OES, and the residue was acid-leached by 0.5 mol L^{-1} citric acid (solid/liquid, 20 g L^{-1}) to recover transition metals at 90 °C for 80 min. The solution was filtered, and the transition metal concentration was measured by ICP-OES. The leaching efficiency was determined by eqn (1):

$$\text{Leaching efficiency} = \frac{C \times V}{m \times W} \quad (1)$$

where C *is* the concentration (g L^{-1}) of the targeted metal in the leaching solution, V is the volume (L) of the acid solution, m is the mass (g) of roasting powder, and W is the mass fraction (%) of the targeted metal in the roasting powder.

2.3 Analysis

The microscopic morphology and particle size of the samples were characterized using SEM (SU-70, Hitachi). The phase composition of the samples was analyzed by XRD with a scanning range (2θ) of 5–80° and a Cu Kα radiation source (40 kV, 100 mA). The surface bonding properties of the samples were investigated by XPS (ESCALAB 250Xi, Thermo Fisher Scientific Inc., USA), with the C_{1s} signal (284.8 eV) used as an internal standard.

The pyrolysis behavior of LNCM and the cathode foil was evaluated by TG (STA449 F3, NETZSCH, Germany). 50 mg of the sample was loaded into an Al_2O_3 crucible under a constant gas flow rate of 10 mL min^{-1}. The analysis was carried out with a heating rate of 10 °C min^{-1} over a temperature range of 30–850 °C.

3. Results and discussion

3.1 XRD analysis and leaching analysis

Previous research has demonstrated that the reduction roasting process is an effective method for recovering valuable metals from the roasting products of LIBs, as it facilitates the formation of water-soluble Li_2CO_3, which can be selectively recovered *via* water leaching.[22,37] Transition metals can subsequently be recovered through chemical approaches, such as acid leaching[15,38] and ammonia leaching,[16] or physical methods, including magnetic separation[30] and flotation.[37,39] Commonly employed reduction methods involve hydrogen reduction and carbothermal reduction. Carbothermal reactions predominantly occur within the temperature range of 600 °C to 800 °C, with the optimal temperature generally centered around 650 °C.[16,22,38,40] In comparison to carbothermal reduction, hydrogen reduction can achieve the reduction of metals at lower temperatures.[20,41] In order to analyze the reduction roasting reaction behavior of samples at different temperatures, the cathode foil and LNCM were subjected to roasting under a pyrolysis gas atmosphere, respectively.

Fig. 2a and b present the XRD patterns of roasting residue of cathode foil ($LiNi_{0.65}Co_{0.15}Mn_{0.2}O_2$) and spent LNCM cell at different temperatures under pyrolysis gas atmosphere. The XRD pattern of the cathode foil exhibited characteristic peaks corresponding to the hexagonal α-$NaFeO_2$ layered structure, appearing at approximately 2θ = 18.7°, 36.66°, 44.34°, 48.52°, and 58.57°, which were assigned to the diffraction planes (003), (101), (104), (105), and (107), respectively (JCPDS no. 09-0063).[42,43] The XRD pattern of the cathode foil and spent LNCM cell at 350 °C both showed weak diffraction peaks of $LiNi_{0.65}Co_{0.15}Mn_{0.2}O_2$, indicating that $LiNi_{0.65}Co_{0.15}Mn_{0.2}O_2$ does not fully decompose at this temperature. The diffraction peaks at 2θ = 37.09°, 43.16°, and 62.66° were attributed to the (111), (200), and (220) crystal planes of NiO, respectively. When the temperature was further increased to 450 °C, $LiNi_{0.65}Co_{0.15}Mn_{0.2}O_2$ was completely reduced, and diffraction peaks corresponding to Li_2CO_3, Ni, NiO, and Co were observed. This suggested that $LiNi_{0.65}Co_{0.15}Mn_{0.2}O_2$ can be effectively reduced under pyrolysis gas atmosphere using CO and H_2 as reductants at a relatively low temperature (450 °C), which is lower than that required for carbothermal reduction (>600 °C)[22] and comparable to hydrogen reduction.[41]

The roasting products of the cathode foil and spent LNCM cell were significantly different when the roasting temperatures were above 450 °C. At 550 °C, the diffraction peak of MnO appeared in the roasting products of the cathode foil; and the diffraction peak of NiO disappeared at 750 °C, and only Ni, Co, Al, and MnO were detected (Fig. 2a). However, at this temperature, the characteristic peak of water-insoluble $LiAlO_2$ also appeared simultaneously. In comparison, LNCM cells required a lower temperature to achieve the complete reduction of cathode materials. For instance, the characteristic peaks of MnO could be observed at 450 °C, and when the temperature rose to 550 °C, NiO was completely reduced to Ni, accompanied by the generation of $LiAlO_2$ (Fig. 2b). As the roasting temperature further increased, the intensities of the diffraction peaks corresponding to Ni, Co, MnO, and $LiAlO_2$ gradually increased. Meanwhile, the intensity of the Li_2CO_3 peaks tended to weaken, indicating that reactions between Li_2O and the Al foil occurred. Thermodynamically, LNCM can decompose into Li_2O, NiO, CoO, and MnO through carbothermal reduction and gas reduction at high temperatures (reaction (2)).[30] Li_2O can react with CO_2 or CO to form Li_2CO_3 (reactions (3)–(4)) or react with Al to form $LiAlO_2$ (reaction (5)) under favorable thermodynamic conditions. Meanwhile, NiO and CoO can be further reduced to metallic Ni and Co at elevated temperatures (>550 °C) under the reducing influence of carbon, H_2, and CO (reactions (6)–(11)). This is due to the negative ΔG^{θ} values of these reactions, which indicate that they proceed spontaneously under such thermal conditions.

$$LiNi_{0.65}Co_{0.15}Mn_{0.2}O_2 \rightarrow Li_2O + NiO + CoO + MnO + O_2 \quad (2)$$

$$Li_2O + CO_2(g) \rightarrow Li_2CO_3, \quad \Delta G^{\theta}_T = 0.130T - 207.6 \text{ kJ mol}^{-1} \quad (3)$$

$$Li_2O + 2CO(g) \rightarrow Li_2CO_3 + C, \quad \Delta G^{\theta}_T = 0.311T - 298.93 \text{ kJ mol}^{-1} \quad (4)$$

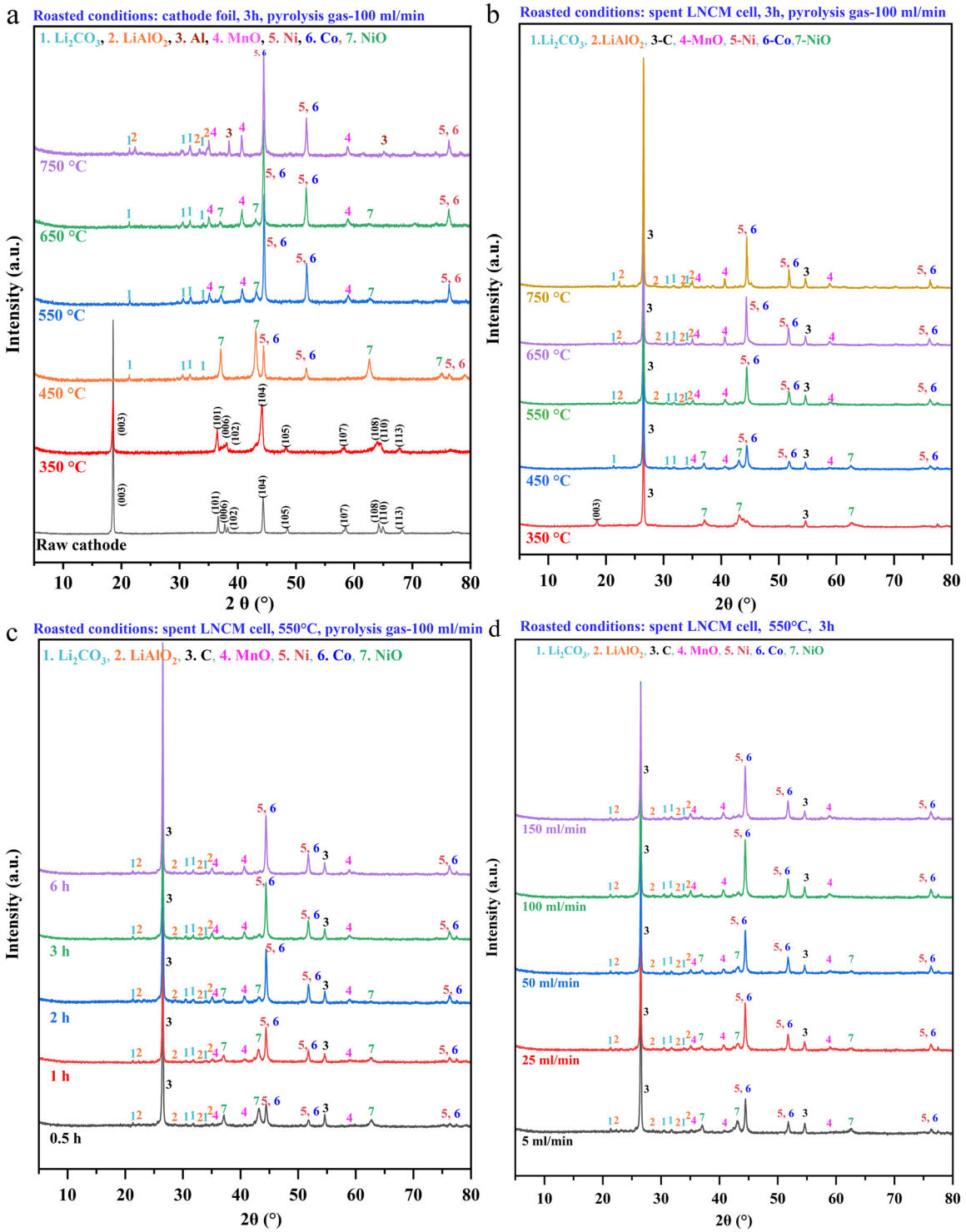

Fig. 2 XRD patterns of roasting residue under different roasting conditions. Cathode foil (a) and spent LNCM cell (b) with pyrolysis gas at different temperatures; (c) spent LNCM cell with pyrolysis gas at different time; (d) spent LNCM cell with pyrolysis gas at different gas flow rates.

$$Li_2O + Al_2O_3(g) \rightarrow 2LiAlO_2, \quad \Delta G_T^\theta = -0.018T - 108.89 \text{ kJ mol}^{-1} \quad (5)$$

$$H_2(g) + NiO \rightarrow H_2O(g) + Ni, \quad \Delta G_T^\theta = -0.035T - 8.73 \text{ kJ mol}^{-1} \quad (6)$$

$$H_2(g) + CoO \rightarrow H_2O(g) + Co, \quad \Delta G_T^\theta = -0.018T - 11.49 \text{ kJ mol}^{-1} \quad (7)$$

$$CO(g) + NiO \rightarrow CO_2(g) + Ni, \quad \Delta G_T^\theta = -0.012T - 43.50 \text{ kJ mol}^{-1} \quad (8)$$

$$CO(g) + CoO \rightarrow CO_2(g) + Co, \quad \Delta G_T^\theta = -0.017T - 48.99 \text{ kJ mol}^{-1} \quad (9)$$

$$C + 2NiO \rightarrow CO_2(g) + 2Ni, \quad \Delta G_T^\theta = -0.178T - 79.83 \text{ kJ mol}^{-1} \quad (10)$$

$$C + 2CoO \rightarrow CO_2(g) + 2Co, \quad \Delta G_T^\theta = -0.143T - 74.31 \text{ kJ mol}^{-1} \quad (11)$$

$$2C + O_2(g) \rightarrow 2CO_2, \quad \Delta G_T^\theta = -0.002T - 394.47 \text{ kJ mol}^{-1} \quad (12)$$

$$C + CO_2(g) \rightarrow 2CO(g), \quad \Delta G_T^\theta = -0.177T - 124.14 \text{ kJ mol}^{-1} \quad (13)$$

$$CO(g) + H_2O \rightarrow H_2(g) + CO_2(g), \quad \Delta G_T^\theta = -0.033T - 24.69 \text{ kJ mol}^{-1} \quad (14)$$

$$H_2O + C \rightarrow H_2(g) + CO(g), \quad \Delta G_T^\theta = -0.142T + 134.79 \text{ kJ mol}^{-1} \quad (15)$$

The gas compositions of the produced gaseous products at different roasting temperatures are listed in Table 1. The produced gases are primarily composed of CO_2, CO, and H_2, along with trace amounts of alkanes. Generally, $LiNi_{0.65}Co_{0.15}Mn_{0.2}O_2$ decomposes into CoO, NiO, and Li_2O, accompanied by the release of O_2.[30] The corresponding reactions and their associated Gibbs free energy are represented by reactions (3)–(11). The produced O_2 can combine with H_2 and carbon to form H_2O and CO_2 (reaction (12)). Additionally, the hydrogen reduction process of the decomposition products (CoO and NiO) also results in the formation of H_2O. When carbon (graphite) is present in the system, it can react with H_2O to form H_2 and CO at high temperatures.[30] Pyrolysis of the organic materials in the spent LNCM cell is a complex multi-stage process that primarily involves dehydration, dehydrogenation, depolymerization, and decomposition reactions.[44,45] This process generates carbon and volatile components, including H_2, CH_4, CO, CO_2, and tar. Then, some volatile compounds are unstable and can undergo secondary reactions, such as Boudouard reaction (reaction (13)), water gas shift reaction (reaction (14)), and water–gas reaction (reaction (15)), all of which will produce CO and H_2.[46–48] Moreover, previous research showed that Ni could effectively catalyze the Boudouard reaction and the water–gas reaction to generate H_2.[46,49] An increase in roasting temperature leads to a gradual rise in the concentration of CO within the gaseous products, accompanied by a corresponding decrease in the level of CO_2. This trend further supports the occurrence of the Boudouard reaction at elevated temperatures. Therefore, it can be concluded that organic materials in LIBs decompose into gaseous products (CO_2, CO, and H_2) at elevated temperatures, and the reductive gases (CO and H^2) can facilitate the reduction of $LiNi_{0.65}Co_{0.15}Mn_{0.2}O_2$. Additionally, graphite can also serve as a reducing agent for carbothermal reduction. Moreover, the synergistic effect of carbon and reductive gases may facilitate the decomposition of $LiNi_{0.65}Co_{0.15}Mn_{0.2}O_2$ at lower temperatures.[27] Therefore, the reduction-roasting process of spent LNCM incorporating pyrolysis gas holds promise as an environmentally friendly and economically viable method for metal recovery.

Following the reduction roasting of spent LNCM cell, lithium present in the form of Li_2CO_3 in the roasted products was subsequently recovered through water leaching. The remaining residue was then subjected to citric acid leaching for the recovery of Ni, Co, and Mn. The leaching results are presented in Fig. 3. Initially, 13.84% Li, 27.90% Ni, 27.58% Co, and 25.98% Mn could be recovered from spent LNCM using water leaching and acid leaching (Fig. 3b). After roasting, the metal leaching efficiency for cathode foil and spent LNCM cell was significantly increased. Within the examined range of roasting temperatures, the roasting temperature had a substantial impact on the Li leaching efficiency. As the roasting temperature increased from 350 °C to 450 °C, the Li leaching efficiency of the LNCM rose from 36.99% to 81.01%, and further increased to 91.62% when the temperature was raised to 550 °C, which exceeded previous reports (84.7%[38] and 82.2%[16]). Similar to the water leaching of Li, the citric acid leaching efficiencies of transition metals exhibited a similar trend over the examined temperature range. The highest leaching efficiencies for transition metals were achieved at 550 °C, with values of 98.71% (Ni), 99.46% (Co), and 98.51% (Mn), respectively. Fig. S7 showed that the valuable metal materials can be effectively recovered by roasting treatment under pyrolysis gas combined with solution leaching. When the roasting temperature was below 550 °C, the lithium leaching efficiency for the cathode foil was lower than that of the spent LNCM cell (Fig. 3a), while the recovery rates of Ni (99.42%), Co (99.26%), and Mn (97.98%) are comparable to those of the spent LNCM

Table 1 The gas composition for the roasting of spent LNCM cells under pyrolysis gas at different temperatures

	Gas composition/%			
Roasting temperatures	CO_2	CO	H_2	Others
350 °C	70.22	14.06	14.25	1.29
450 °C	71.60	12.90	14.00	1.18
550 °C	72.78	13.63	12.64	0.89
650 °C	69.64	15.92	13.26	0.97
750 °C	62.82	19.72	14.72	2.57

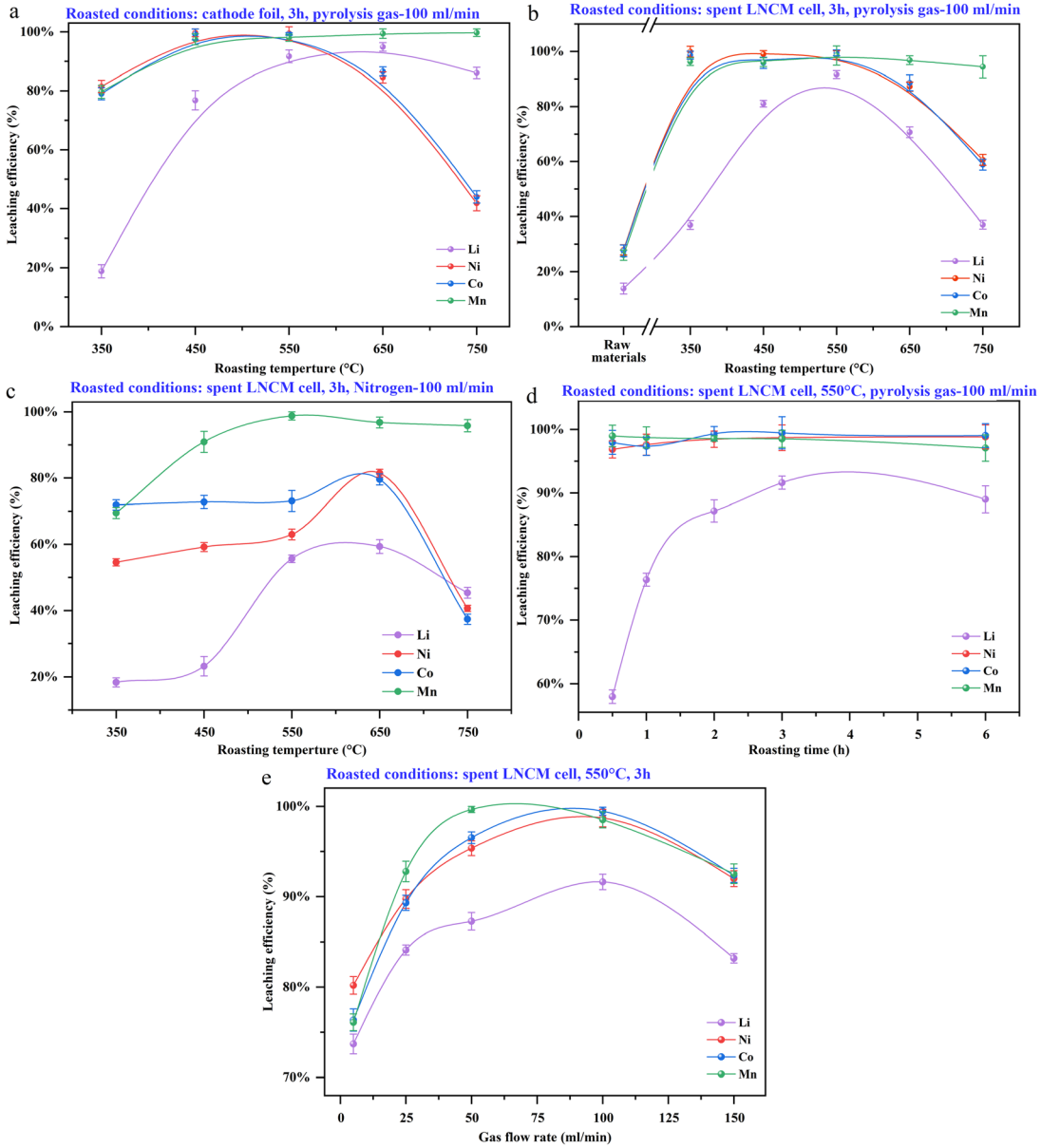

Fig. 3 Effect of roasting conditions on the leaching efficiency of lithium and transition metals (Ni, Co, and Mn) from roasting residue. Cathode foil (a) and spent LNCM cell (b) with pyrolysis gas at different temperatures; (c) spent LNCM cell with N_2 at different temperatures; (d) spent LNCM cell with pyrolysis gas at different time; (e) spent LNCM cell with pyrolysis gas at different gas flow rates.

cell. Notably, both the cathode foil and spent LNCM cell exhibited a significant decrease in metals leaching efficiency, especially lithium, nickel, and cobalt, when the roasting temperature was further increased to 750 °C. Wu *et al.*[50] observed a similar phenomenon during the leaching of transition metals using citric acid. It was found that when the roasting temperature exceeded 600 °C, the leaching efficiency of transition metals exhibited a decreasing trend. This phenomenon might be attributed to the fact that water-insoluble $LiAlO_2$ was easily produced under high-temperature conditions. Meanwhile, water-soluble Li_2CO_3 tends to decompose into water-insoluble Li_2O_2 at temperatures exceeding 700 °C.[51,52] Moreover, the produced nickel and cobalt are prone to recombine and form solid solution alloys at 750 °C, which markedly reduces their susceptibility to acid leaching.[53–55]

In order to assess the actual influence of pyrolysis gas on the roasting process of spent LNCM cell, some control experiments were conducted under a N_2 atmosphere. Furthermore, a comparative analysis was performed on the chemical compositions and metal leaching efficiencies of the roasted products obtained from spent LNCM cell under pyrolysis gas and N_2 atmospheres, respectively. The XRD patterns of the roasting products of spent LNCM cell in an N_2 atmosphere are shown in Fig. S8. The diffraction peaks corresponding to

$LiNi_{0.65}Co_{0.15}Mn_{0.2}O_2$ disappeared completely only when the temperature was increased to 550 °C, while the characteristic peaks of Li_2CO_3, Ni, NiO, and Co were observed. This indicated that the decomposition temperature of LNCM in an inert atmosphere is significantly higher than that in a pyrolysis gas atmosphere. Notably, at 550 °C, NiO was present in the roasting products of spent LNCM cell with N_2 and cathode foil with a gas mixture; however, it disappeared in the roasting products of spent LNCM cell with pyrolysis gas. At 650 °C, the composition of the roasting product of spent LNCM cell under N_2 atmosphere was almost identical to that obtained in a pyrolysis gas atmosphere. However, the characteristic peaks of Li_2CO_3 and NiO disappeared when the temperature was further increased to 750 °C. Moreover, the metal leaching efficiencies of the spent LNCM cell roasting products under a nitrogen atmosphere, especially for lithium, nickel, and cobalt, were significantly lower than those of the roasting products obtained in a pyrolysis gas atmosphere in all roasting temperature ranges (Fig. 3c).

As shown in Fig. 2c, under the roasting conditions of 550 °C and a gas flow rate of 100 ml min^{-1}, the chemical composition of the roasting products remained consistent within the time range of 0.5 to 2 h, including C, Li_2CO_3, $LiAlO_2$, Ni, NiO, Co, and MnO. This suggested that $LiNi_{0.65}Co_{0.15}Mn_{0.2}O_2$ can be fully reduced within 0.5 h. When the roasting time was extended to 3 h, NiO was further reduced to Ni, and the leaching efficiency of Li and transition metals reached its maximum (Fig. 3d). However, upon further prolonging the roasting time to 6 h, the leaching efficiency of Li and transition metals decreased instead.

The influence of gas flow rate on the chemical composition and metal leaching efficiency of spent LNCM cell roasting products was investigated at 550 °C for 3 h. The results are shown in Fig. 2d and Fig. 3e, respectively. When the gas flow rate was within the range of 5 to 50 mL min^{-1}, the diffraction peaks of NiO were still evident in the XRD patterns of the roasting products; however, at a gas flow rate of 100 mL min^{-1}, the characteristic peaks of NiO disappeared, leaving only the characteristic peaks of Ni. As the gas flow rate increased, the leaching efficiencies of the metals gradually improved and reached their maximum values at a gas flow rate of 100 mL min^{-1}. However, when the gas flow rate was further increased, the metal leaching efficiencies slightly declined.

Generally, Nickel and cobalt oxides are classified as basic oxides; the reaction between basic oxides and citric acid is typically an acid–base neutralization reaction, whereas the reaction between metal monomers and citric acid belongs to redox reactions. The reaction rates of acid–base neutralization processes are generally higher than those of redox reactions.[50] Furthermore, due to the weak oxidizing capability of citric acid, its reactivity with elemental nickel and cobalt is relatively limited. Therefore, elevated roasting temperature, prolonged reaction time, and increased gas flow rates can increase the content of Ni and Co monomers in the roasting products, resulting in a reduction in their leaching efficiency. After achieving the optimal reaction conditions, the leaching rate of manganese is less affected by the roasting conditions. This is because within the entire temperature range from 0 to 1000 °C, the reduction reaction of MnO is thermodynamically difficult to occur spontaneously due to the positive ΔG^{θ} value of the reduction of MnO to Mn.[56] Therefore, manganese mainly exists in the form of MnO in the roasting products.

3.2 SEM analysis

The surface morphologies of the cathode foil and the roasting products of spent LNCM cell at different temperatures are presented in Fig. 4. The cathode material exhibited a large number of uniformly and neatly arranged

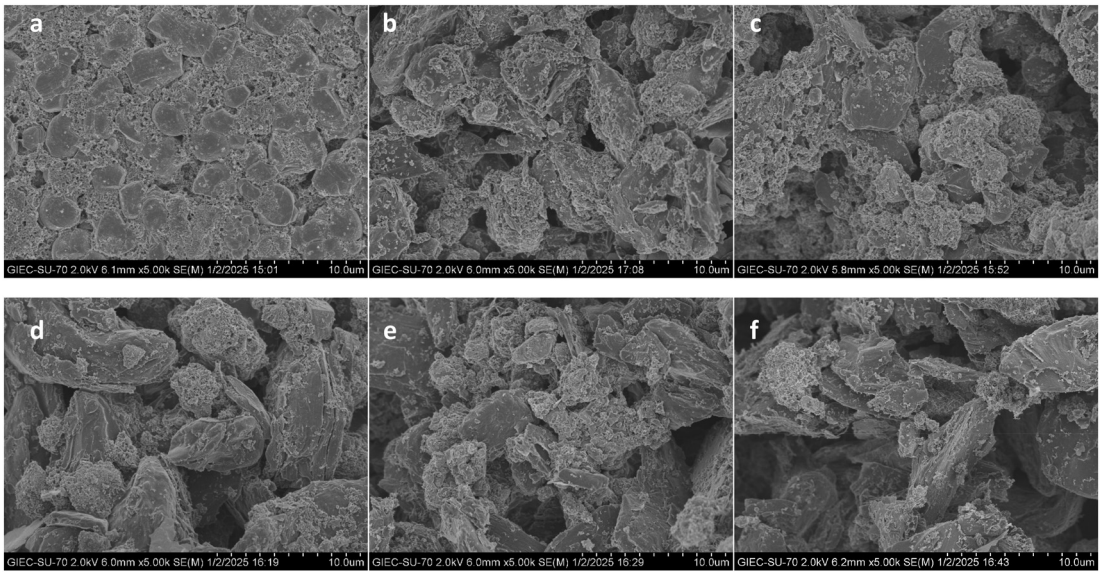

Fig. 4 SEM images of cathode material (a) and roasting residue of spent LNCM cell at 350 °C (b), 450 °C (c), 550 °C (d), 650 °C (e), and 750 °C (f) (roasted conditions: mixture gas atmosphere flow, 100 mL min^{-1}, roasting time 3 h).

$LiNi_{0.65}Co_{0.15}Mn_{0.2}O_2$ particles with a particle size of approximately 2 μm, and C, O, F, Ni, Co, Mn were evenly distributed within these particles (Fig. S1). After roasting treatment, most of the $LiNi_{0.65}Co_{0.15}Mn_{0.2}O_2$ complex remained in the roasting residue at 350 °C because the fluorinated binder was not completely decomposed (Fig. S2), which is consistent with the XRD results. At higher roasting temperatures, $LiNi_{0.65}Co_{0.15}Mn_{0.2}O_2$ decomposed into irregular particles, and numerous cracks appeared on its surface (Fig. S3–S6) due to oxygen evolution during the roasting process. These particles agglomerated on the laminar graphite, and the particle size of the graphite continued to decrease as the temperature increased.

3.3 XPS analysis

Fig. 5 presents the XPS spectra of the cathode foil and the roasting residue of the spent LNCM cell at various temperatures. The cathode foil exhibited characteristic peaks at binding energies (BE) of 856.26 eV (Ni^{3+}), 873.75 eV (Ni^{3+}), 779.58 eV (Co^{3+}), 794.59 eV (Co^{3+}), 796.95 eV (Co^{2+}), and 641.71 eV (Mn^{3+}), which correspond to the high-valence states of Ni, Co, and Mn,[40,57] respectively. The XPS spectra of the roasting products at 350 °C showed characteristic peaks consistent with $LiNi_{0.65}Co_{0.15}Mn_{0.2}O_2$, aligning with the XRD results. When the roasting temperature exceeded 450 °C, new peaks appeared at BE values of 852.31 eV, 778.37 eV, and 640.87 eV, corresponding to Ni^0, Co^0, and Mn^{2+},[41] respectively. This indicates that the high-valence states of metals (Ni^{3+}, Co^{3+}, and Mn^{3+}) were successfully reduced to lower-valence states such as Ni^{2+}/Ni, Co^{2+}/Co, and Mn^{2+} through roasting pre-treatment under a pyrolysis gas atmosphere.

3.4 Synergetic effect analysis

To further investigate the potential synergistic effect between gas reduction and carbon reduction, the TG analysis was performed on the samples under both inert and pyrolysis gas atmospheres, aiming to analyze the physical and chemical transformations occurring at various temperatures, and the TG-DTG curves of the cathode foil and LNCM are shown in

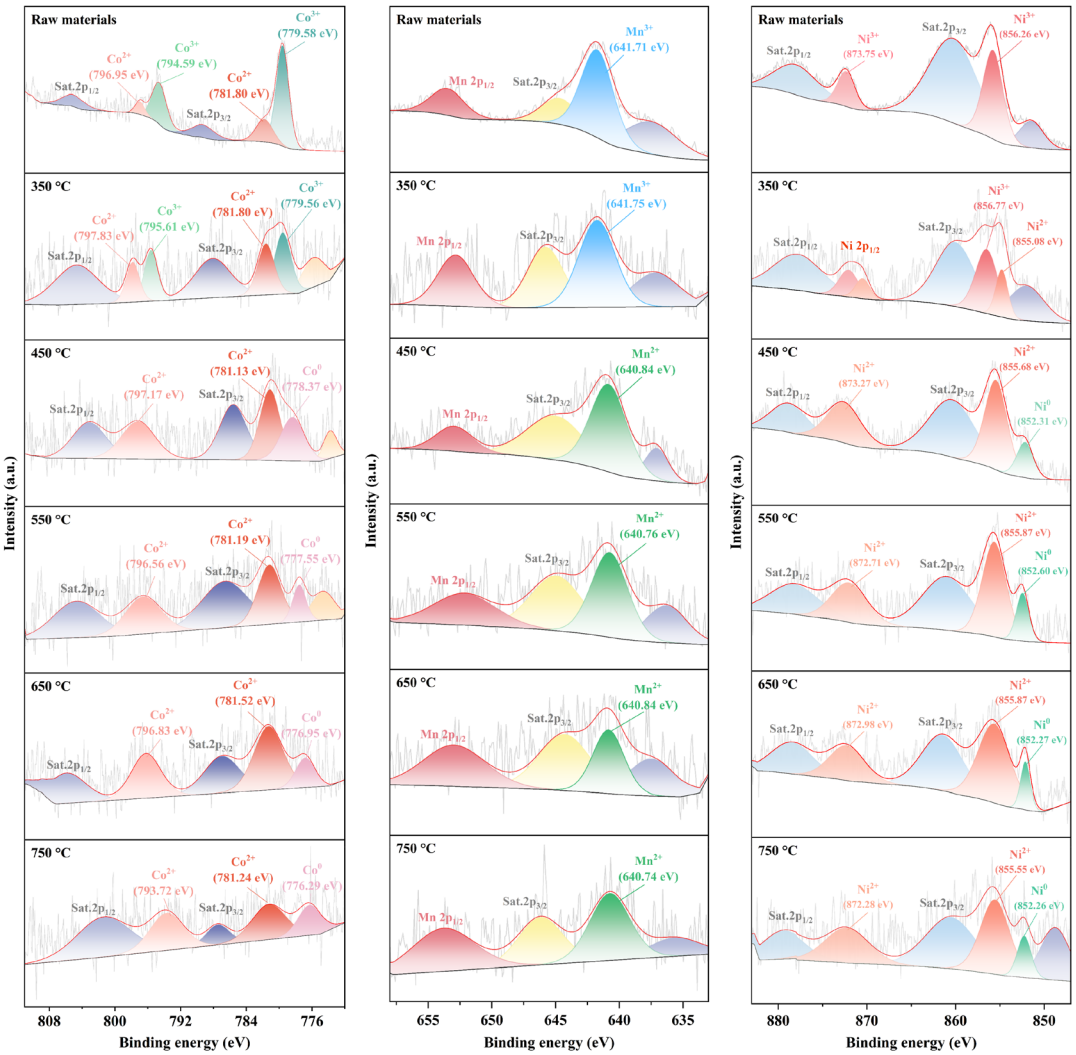

Fig. 5 XPS spectra of cathode material and roasting residue of spent LNCM cell at different roasted temperatures. (left) Ni 2p; (center) Co 2p; (right) Mn 2p.

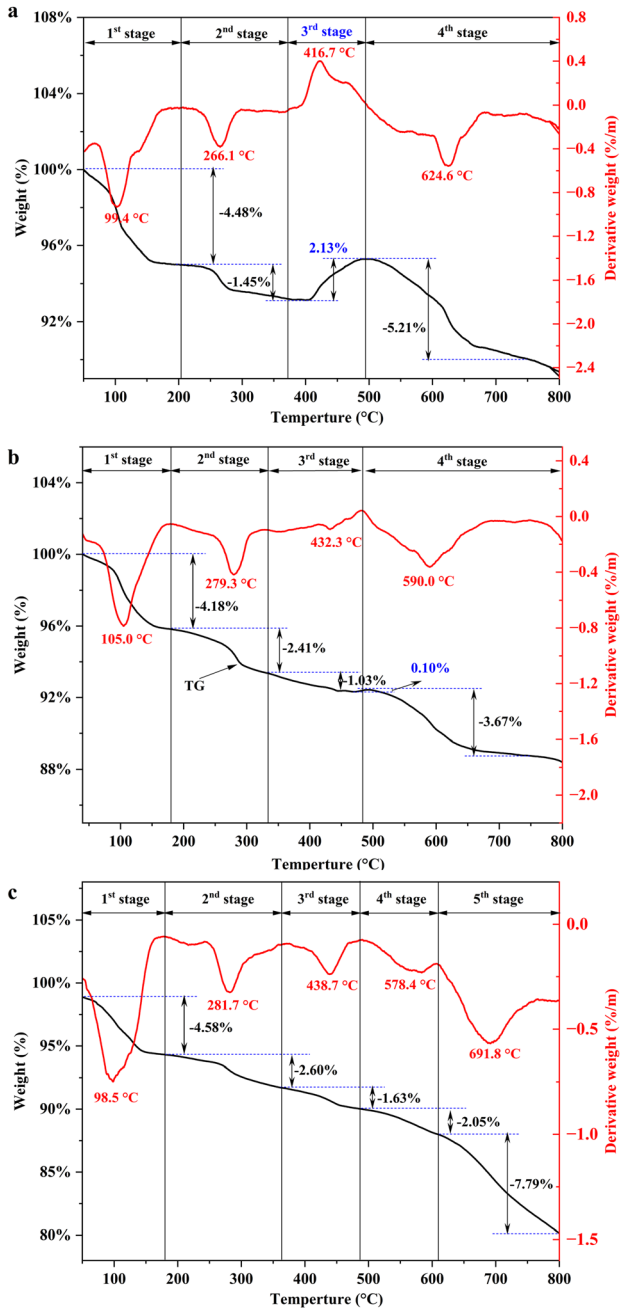

Fig. 6 TG and TDG curves of the cathode foil with mixture gas (a), spent LNCM cell with pyrolysis gas (b), and spent LNCM cell with Ar (c).

Fig. 6. The pyrolysis process of the cathode foil under a pyrolysis gas atmosphere (Fig. 6a) can be divided into four distinct stages: in the first stage (<204 °C), the volatilization of organic electrolytes and/or water occurs, resulting in a mass loss rate of 4.48%.[58] Typically, freshly stripped cathode foil contains a significant amount of residual electrolyte, and a trace amount of water may be adsorbed during sample preparation. The temperature of maximum weight loss rates (T_{max}) at 99.4 °C indicates rapid desorption of water and electrolytes at this temperature. The second stage occurs between 204 °C and 372 °C, with a mass loss of 1.45%, which is mainly due to the partial $LiNi_{0.65}Co_{0.15}Mn_{0.2}O_2$ being decomposed into CoO, NiO, and Li_2O, and releasing O_2. In the third stage (372 °C–493 °C), there is no mass loss but rather a slight mass gain of 2.13%, which can be caused by carbonation of Li_2O with CO or CO_2 to form Li_2CO_3.[20,59] The fourth stage (>493 °C), characterized by a T_{max} at 624.6 °C, which corresponds to the degradation of organic binders and the reduction of metallic compounds, leading to the formation of a large amount of small-molecule volatile products and resulting in a mass loss rate of 5.21%.[60] The organic binders decompose into carbon, fluorobenzene, and HF.[61] The small amount of HF and fluorobenzene in the gaseous products can be effectively absorbed by water. The reduction of CoO and NiO to Co and Ni occurs during this stage, indicating that the produced CoO and NiO are further reduced by pyrolysis gases (H_2 and CO) to form Co and Ni. These results are consistent with the XRD patterns of the spent LNCM cell roasting products.

In Fig. 6b, the weight loss trend of the spent LNCM cell is consistent with that of the cathode foil under a pyrolysis gas atmosphere, both exhibiting four-stage reactions. The mass loss of LNCM primarily occurs in four temperature ranges: 80 °C–180 °C, 200 °C–330 °C, 350 °C–490 °C, and 500 °C–700 °C, with corresponding mass losses of 4.18%, 2.41%, 1.02%, and 3.67%, respectively. These temperature intervals mainly correspond to four stages: the removal of electrolyte or adsorbed water, the decomposition of the separator, the reduction of cathode materials accompanied by carbonation of the Li_2O, and the carbothermal reduction stage coupled with binder decomposition. The T_{max} of the spent LNCM cell in the DTG curve is higher than that of the cathode foil in the first three stages. However, in the fourth stage, the T_{max} of the spent LNCM cell (590 °C) is significantly lower than that of the cathode foil (624.6 °C). Compared with the cathode foil, the spent LNCM cell contains the separator and graphite, resulting in a relatively higher T_{max} during the first three stages. In the fourth stage, the lower T_{max} indicates that there is a significant synergistic reduction effect between the reductive gases in the pyrolysis gas and the carbon resource, which can promote both the degradation of the binder and the reduction of the LNCM decomposition products (CoO and NiO), thereby accelerating the reaction rate and leading to an earlier maximum decomposition temperature.

Fig. 6c presents the TG and DTG curves of spent LNCM cell under an argon atmosphere. The DTG curve displays five distinct T_{max} at 98.5 °C, 281.7 °C, 438.7 °C, 578.4 °C, and 749.17 °C, corresponding to the volatilization of the electrolyte,[21] gasification of the separator, decomposition of $LiNi_{0.65}Co_{0.15}Mn_{0.2}O_2$, reduction of cathode materials, and gasification of the binder, respectively. During the pyrolysis process, the electrolyte volatilizes first as the temperature increases, followed by the separator, cathode material, and binders. Notably, in the later stages of pyrolysis (above 200 °C), the T_{max} of the spent LNCM cell under an inert atmosphere in the DTG curve is significantly higher than that under a pyrolysis gas atmosphere. Additionally, no weight gain was observed

within the temperature range of 400 to 500 °C, which can be attributed to the relatively low concentrations of CO and CO_2 in the system, resulting in insufficient formation of Li_2CO_3.

The XPS spectra of the residue from spent LNCM cell with N_2 (Fig. 7) exhibit peaks at binding energies (BE) of 856.56 eV (Ni^{3+}) and 779.18 eV (Co^{3+}), indicating that some higher-valence metals remain unreduced, thereby reducing the metal leaching efficiency. This suggests that carbothermal reduction alone is insufficient to fully convert $LiNi_{0.65}Co_{0.15}Mn_{0.2}O_2$ into readily leachable metals. In contrast, the XPS spectra of the residue from the cathode foil with pyrolysis gas (Fig. 7) show only the presence of Ni^0, Co^0, and Mn^{2+}, similar to the results

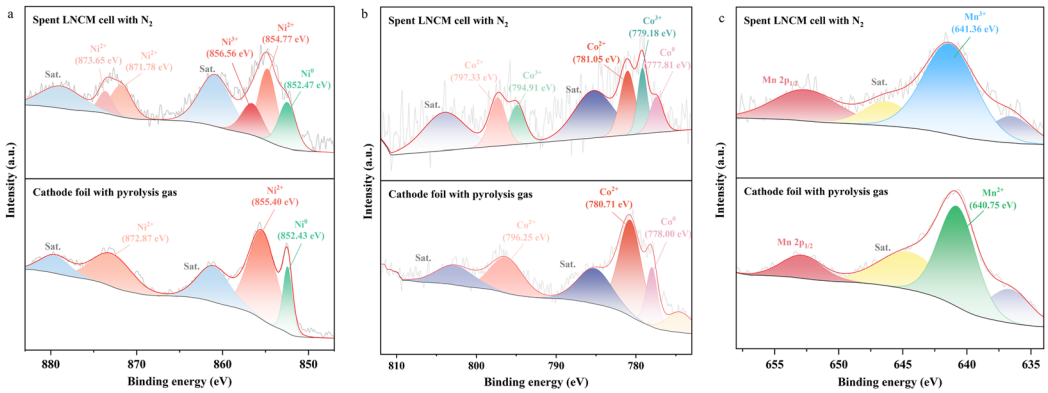

Fig. 7 The XPS spectra of the residue of the spent LNCM cell with N_2 and cathode foil with pyrolysis gas at 550 °C. Ni 2p (a), Co 2p (b), and Mn 2p (c).

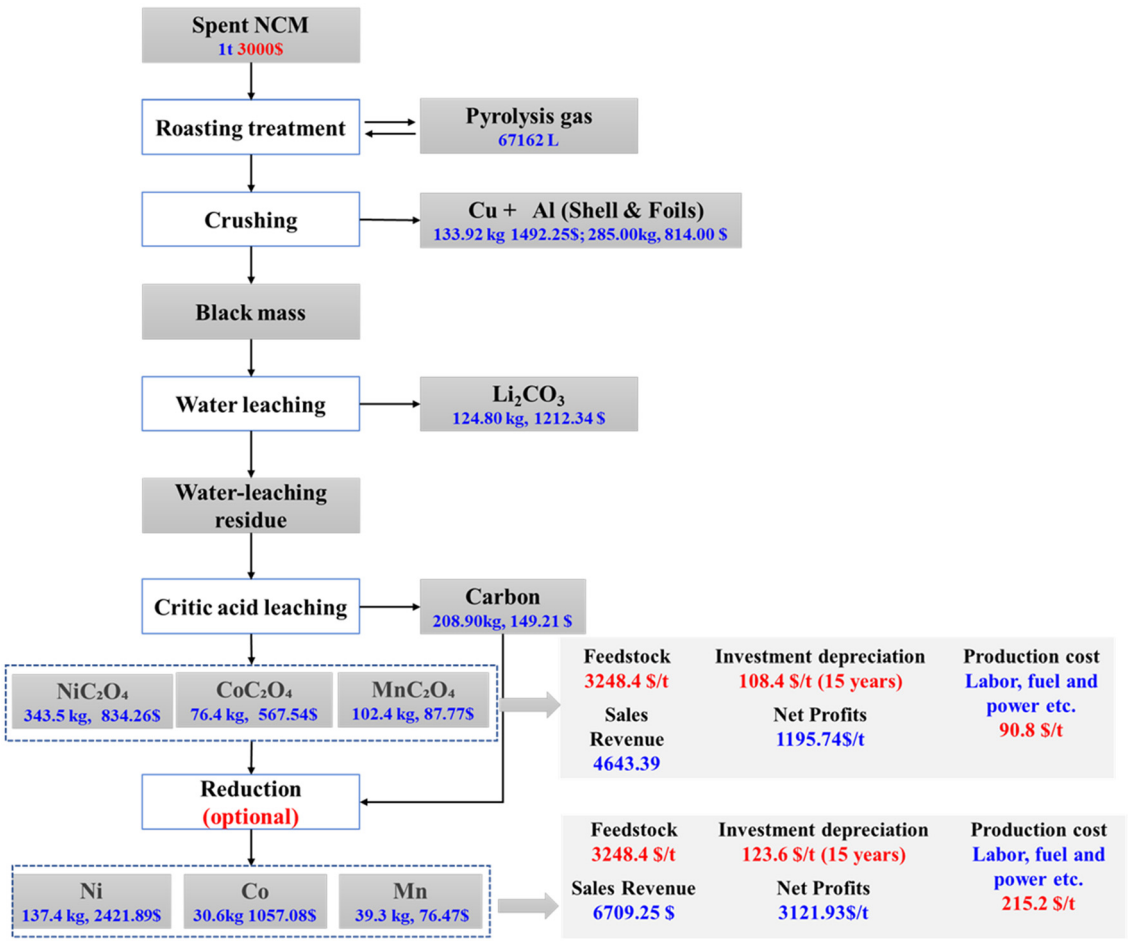

Fig. 8 Economic evaluation of the proposed roasting reduction method for recovering valuable metals from spent LIBs by repurposing the pyrolysis gas of the LIBs.

observed for the spent LNCM cell with pyrolysis gas. Furthermore, the Fig. 3 also showed that the lithium leaching efficiency for the cathode foil with pyrolysis gas is lower than that of spent LNCM cell when the roasting temperature <550 °C, while the recovery rates of Li (91.68%), Ni (99.42%), Co (99.26%), and Mn (97.98%) are comparable to those of spent LNCM cell under pyrolysis gas atmosphere at 550 °C, but significantly higher than those of spent LNCM cell with N_2 (Fig. 3c, 55.65% of Li, 62.98% of Ni, 73.07% of Co, and 98.76% of Mn). Therefore, it can be concluded that the synergistic reduction effect between the reducing gases in the pyrolysis gas and carbon (graphite) effectively promotes the decomposition of $LiNi_{0.65}Co_{0.15}Mn_{0.2}O_2$, while also reducing the energy consumption associated with the spent LNCM roasting process.

3.5 Economic analysis

A preliminary economic evaluation was carried out for a recycling company in China that processes 10 000 tons per year of spent NCM batteries using the proposed method. All reagent and product prices are based on the up-to-date data available online. Detailed information is provided in Fig. 8. The total project investment amounts to 16.26 million US dollars, covering core equipment, supporting and preprocessing equipment, infrastructure and civil works, as well as other one-time expenses (refer to Table S1). The total cost is $3447.60 per ton, including expenditures on raw materials, chemical reagents, fuel and power consumption, water treatment, labor, and fixed asset depreciation. The primary products include Li_2CO_3 (124.80 kg t^{-1}), copper (133.92 kg t^{-1}), aluminum (285.00 kg t^{-1}), recycled graphite (208.90 kg t^{-1}), metal salts (nickel, 343.52 kg t^{-1}; cobalt, 76.40 kg t^{-1}; and manganese, 102.40 kg t^{-1}), and 67, 162 L of pyrolysis gases. The proposed recycling process generates a unit revenue of $4643.39 per ton, with a corresponding unit net income of $1195.79 per ton. The static investment payback period is 1.36 years, and the static investment return rate is 73.54%. Therefore, the recycling method proposed in this study demonstrates strong economic viability. Furthermore, since the pyrolysis gas contains a significant quantity of reducing gases such as H_2 and CO, the metal salts can be further reduced to metallic elements through reduction reactions, thereby substantially improving the project's investment return rate. It is important to note, however, that these results are derived solely from laboratory-scale experiments. In real-world production scenarios, additional costs such as taxation, procurement, and storage costs must also be considered.

Compared with existing recycling technologies such as hydrometallurgy, pyrometallurgy, and carbothermal reduction, the recycling method proposed in this study offers several notable advantages. Firstly, the process is simple, as it directly utilizes spent NCM batteries as raw materials, thereby eliminating the need for labor-intensive dismantling and binder removal steps commonly required in traditional processes. Secondly, the operating conditions are relatively mild, with an energy consumption of 525 MJ t^{-1}, which represents a 16% reduction compared to the carbothermal reduction process (625 MJ t^{-1}) and amounts to only 35% of the pyrometallurgy process. Finally, no external reducing agents such as biomass are required, as the method efficiently exploits the endogenous carbon sources present in waste NCM materials, thereby further reducing the overall processing cost.

4. Conclusions

The roasting reduction technology for recovering valuable metals from spent LNCM batteries by utilizing the pyrolysis gas generated during thermal decomposition of LIBs has been demonstrated to be an environmentally friendly and economically viable method for LIB recycling at lower temperatures. In this study, the spent LNCM cell, without disassembling or crushing, are roasted at 550 °C under their pyrolysis gas atmosphere. Through the roasting reduction process, the high-valence states of Ni^{3+}, Co^{3+}, and Mn^{3+} in $LiNi_{0.65}Co_{0.15}Mn_{0.2}O_2$ are reduced to Ni^{2+}/Ni, Co^{2+}/Co, and Mn^{2+}, respectively. Additionally, water-soluble Li_2CO_3 is produced, facilitating subsequent metal leaching processes. A recovery rate of 91.62% for lithium is achieved *via* water leaching of the roasting residue, while 98.71% of nickel, 99.46% of cobalt, and 98.51% of manganese are recovered through critic acid leaching of the water-extraction residue. These recovery rates exceed those obtained using carbothermal reduction with carbon-based materials in an inert atmosphere. The synergistic effect between the reductive gases in the pyrolysis gas and the carbon resource is identified as a critical factor enabling the reduction of LNCM at lower temperatures. Consequently, the low-temperature reduction roasting treatment of LNCM before the leaching process can not only effectively improve the leaching efficiency of metal elements but also avoid the use of chemical reductants, thus significantly reducing the risk of environmental pollution.

Author contributions

Zhen Xiong: investigation, wrote the original draft, and formal analysis. Hairong Zhang: conceptualization, review & editing, economic analysis, funding acquisition, and supervision. Can Wang: economic analysis. Haijun Guo: data curation. Mengkun Wang, Hailong Li, Xuefang Chen, and Xiong Lian contributed to the analysis and discussion. Xinde Chen: resources, funding acquisition, and project administration.

Conflicts of interest

There are no conflicts to declare.

Data availability

All relevant data are within the manuscript and its SI. Supplementary information: Fig. S1: SEM-EDS analysis of the

pure $LiNi_{0.65}Co_{0.15}Mn_{0.2}O_2$; Fig. S2–S6: SEM-EDS analysis of the roasting product of LNCM at the range of 350–750 °C under a pyrolysis gas atmosphere; Fig. S7: the XRD patterns of the roasting residue of LNCM (a), water-leaching residue (b), and acid-leaching residue (c); Fig. S8: the XRD pattern of the roasting residue of LNCM with N_2 at different temperatures. Table S1: investment summary. See DOI: **https://doi.org/10.1039/d5gc03423j**.

Acknowledgements

The authors are grateful for the support provided by the Jiangsu Provincial Key Research and Development Program (BE2023078), the Joint Fund of Yulin University and the Dalian National Laboratory for Clean Energy (YLU-DNL Fund 2023002), and the Guangdong Basic and Applied Basic Research Foundation (2022A1515012570).

References

1 F. Wu, J. Maier and Y. Yu, *Chem. Soc. Rev.*, 2020, **49**, 1569–1614.
2 W. Liu, Z. Zheng, Y. Zhang, X. Zhao, Z. Fu, J. Ye, X. Li, Y. Li and C. Hu, *J. Alloys Compd.*, 2023, **963**, 171130.
3 E. Fan, L. Li, Z. Wang, J. Lin, Y. Huang, Y. Yao, R. Chen and F. Wu, *Chem. Rev.*, 2020, **120**, 7020–7063.
4 J. Wang, J. Ma, Z. Zhuang, Z. Liang, K. Jia, G. Ji, G. Zhou and H.-M. Cheng, *Chem. Rev.*, 2024, **124**, 2839–2887.
5 W. Mrozik, M. A. Rajaeifar, O. Heidrich and P. Christensen, *Energy Environ. Sci.*, 2021, **14**, 6099–6121.
6 E. Asadi Dalini, G. Karimi, S. Zandevakili and M. Goodarzi, *Miner. Process. Extr. Metall. Rev.*, 2020, **42**, 451–472.
7 Y. Yang, E. G. Okonkwo, G. Huang, S. Xu, W. Sun and Y. He, *Energy Storage Mater.*, 2021, **36**, 186–212.
8 Y. Tang, H. Xie, B. Zhang, X. Chen, Z. Zhao, J. Qu, P. Xing and H. Yin, *Waste Manage.*, 2019, **97**, 140–148.
9 J. Xu, H. R. Thomas, R. W. Francis, K. R. Lum, J. Wang and B. Liang, *J. Power Sources*, 2008, **177**, 512–527.
10 J. Heelan, E. Gratz, Z. Zheng, Q. Wang, M. Chen, D. Apelian and Y. Wang, *JOM*, 2016, **68**, 2632–2638.
11 W. Wu, X. Liu, X. Zhang, X. Li, Y. Qiu, M. Zhu and W. Tan, *J. Biosci. Bioeng.*, 2019, **128**, 344–354.
12 Y. Xin, X. Guo, S. Chen, J. Wang, F. Wu and B. Xin, *J. Cleaner Prod.*, 2016, **116**, 249–258.
13 W. Gao, X. Zhang, X. Zheng, X. Lin, H. Cao, Y. Zhang and Z. Sun, *Environ. Sci. Technol.*, 2017, **51**, 1662–1669.
14 S. Agarwal, S. Dhiman and H. Gupta, *Environ. Sci. Pollut. Res.*, 2024, **31**, 34249–34257.
15 L. M. J. Rouquette, M. Petranikova and N. Vieceli, *Sep. Purif. Technol.*, 2023, **320**, 124143.
16 Y. Ma, J. Tang, R. Wanaldi, X. Zhou, H. Wang, C. Zhou and J. Yang, *J. Hazard. Mater.*, 2021, **402**, 123491.
17 G. Siyu, D. Enhua, L. Bingguo, Y. Chao, N. Yifan, J. Guangxiong, C. Wang, H. Keren, G. Shenghui and Z. Libo, *Sep. Purif. Technol.*, 2024, **348**, 127771.
18 X. Chen, C. Luo, J. Zhang, J. Kong and T. Zhou, *ACS Sustainable Chem. Eng.*, 2015, **3**, 3104–3113.
19 V. Srivastava, V. Rantala, P. Mehdipour, T. Kauppinen, S. Tuomikoski, A. Heponiemi, H. Runtti, P. Tynjälä, G. Simões Dos Reis and U. Lassi, *Chem. Eng. J.*, 2023, **474**, 145822.
20 F. Xie, C. Wang, Y. Sun, Y. Fan, Z. Zhao and Y. Yao, *Sep. Purif. Technol.*, 2023, **318**, 123972.
21 Y. Zhao, B. Liu, L. Zhang and S. Guo, *J. Hazard. Mater.*, 2020, **396**, 122740.
22 F. Zhou, J. Ma, H. Wang, M. Cai, X. Qu, J. Zhao, D. Wang, Y. Cai, D. Wang and H. Yin, *J. Hazard. Mater.*, 2024, **477**, 135304.
23 H. Pinegar, R. Marthi, P. Yang and Y. R. Smith, *ACS Sustainable Chem. Eng.*, 2021, **9**, 7447–7453.
24 W. Gao, C. Liu, H. Cao, X. Zheng, X. Lin, H. Wang, Y. Zhang and Z. Sun, *Waste Manage.*, 2018, **75**, 477–485.
25 B. Makuza, Q. Tian, X. Guo, K. Chattopadhyay and D. Yu, *J. Power Sources*, 2021, **491**, 229622.
26 P. Liu, L. Xiao, Y. Tang, Y. Chen, L. Ye and Y. Zhu, *J. Therm. Anal. Calorim.*, 2019, **136**, 1323–1332.
27 M. A. Hasan, R. Hossain and V. Sahajwalla, *Green Chem.*, 2025, **27**, 1073–1088.
28 T. Zhao, W. Li, M. Traversy, Y. Choi, A. Ghahreman, Z. Zhao, C. Zhang, W. Zhao and Y. Song, *J. Environ. Manage.*, 2024, **351**, 119670.
29 C. Pan and Y. Shen, *J. Energy Chem.*, 2023, **85**, 547–561.
30 Q. Peng, X. Zhu, J. Li, Q. Liao, Y. Lai, L. Zhang, Q. Fu and X. Zhu, *Waste Manage.*, 2021, **134**, 100–109.
31 X. Zhong, W. Liu, J. Han, F. Jiao, W. Qin and T. Liu, *J. Cleaner Prod.*, 2020, **263**, 121439.
32 P. Handel, G. Fauler, K. Kapper, M. Schmuck, C. Stangl, R. Fischer, F. Uhlig and S. Koller, *J. Power Sources*, 2014, **267**, 255–259.
33 J. Lee, K. W. Park, I. Sohn and S. Lee, *Int. J. Miner., Metall. Mater.*, 2024, **31**, 1554–1571.
34 R. Tao, P. Xing, H. Li, Z. Sun and Y. Wu, *Resour., Conserv. Recycl.*, 2022, **176**, 105921.
35 Y. Ni, N. Chun-Chen, L. Xian-Jun, R. Yang-Guang and X.-N. Zhu, *Energy Sources, Part A*, 2023, **45**, 10242–10259.
36 Y. Shin, S. Kim, S. Park, J. Lee, J. Bae, D. Kim, H. Joo, S. Ban, H. Lee, Y. Kim and K. Kwon, *Renewable Sustainable Energy Rev.*, 2023, **187**, 113693.
37 G. Zhang, Y. He, Y. Feng, H. Wang and X. Zhu, *ACS Sustainable Chem. Eng.*, 2018, **6**, 10896–10904.
38 J. Hu, J. Zhang, H. Li, Y. Chen and C. Wang, *J. Power Sources*, 2017, **351**, 192–199.
39 G. Hong, H. Park, A. Gomez-Flores, H. Kim, J. Lee and J. Lee, *Sep. Purif. Technol.*, 2024, **336**, 126327.
40 W. Liu, Q. Qin, H. Zhang, W. Zhao, X. Chen, J. Xiong, Y. Han, S. Zheng, C. Zhang, G. Li and P. Li, *Waste Manage.*, 2024, **187**, 119–127.
41 G. S. Bhandari and N. Dhawan, *J. Sustain. Metall.*, 2022, **8**, 1704–1718.

42 L. You, Y. Wen, G. Li, B. Chu, J. Wu, T. Huang and A. Yu, *J. Mater. Chem. A*, 2022, **10**, 5631–5641.
43 L. Cheng, B. Zhang, S.-L. Su, L. Ming, Y. Zhao and X.-X. Tan, *J. Solid State Chem.*, 2021, **297**, 122045.
44 F.-X. Collard and J. Blin, *Renewable Sustainable Energy Rev.*, 2014, **38**, 594–608.
45 T. Kan, V. Strezov and T. J. Evans, *Renewable Sustainable Energy Rev.*, 2016, **57**, 1126–1140.
46 J. Wang, B. Zhao, S. Liu, D. Zhu, F. Huang, H. Yang, H. Guan, A. Song, D. Xu, L. Sun, H. Xie, W. Wei, W. Zhang and T. Pedersen, *Energy Convers. Manage.*, 2022, **254**, 115246.
47 M. K. Karmakar and A. B. Datta, *Bioresour. Technol.*, 2011, **102**, 1907–1913.
48 Ö. Tezer, N. Karabağ, A. Öngen, C. Ö. Çolpan and A. Ayol, *Int. J. Hydrogen Energy*, 2022, **47**, 15419–15433.
49 B. Abdullah, N. A. Abd Ghani and D.-V. N. Vo, *J. Cleaner Prod.*, 2017, **162**, 170–185.
50 X. Wu, J. Tang, Y. Sun and Y. Zhou, *JOM*, 2024, **76**, 1576–1586.
51 A. S. Amarasekara and A. B. Shrestha, *J. Anal. Appl. Pyrolysis*, 2024, **179**, 106471.
52 T. Takahashi and H. Watanabe, *Fusion Eng. Des.*, 1989, **8**, 399–405.
53 Y.-K. Sun, S.-T. Myung, B.-C. Park, J. Prakash, I. Belharouak and K. Amine, *Nat. Mater.*, 2009, **8**, 320–324.
54 J. Zheng, P. Yan, L. Estevez, C. Wang and J.-G. Zhang, *Nano Energy*, 2018, **49**, 538–548.
55 A. Manthiram, J. C. Knight, S.-T. Myung, S.-M. Oh and Y.-K. Sun, *Adv. Energy Mater.*, 2016, **6**, 1501010.
56 Z. Xiong, H. Zhang, H. Guo, M. Wang, C. Wang, H. Li, L. Xiong, X. Chen and X. Chen, *Sustainable Energy Fuels*, 2025, **9**, 3023–3033.
57 P. Liu, L. Xiao, Y. Chen, Y. Tang, J. Wu and H. Chen, *J. Alloys Compd.*, 2019, **783**, 743–752.
58 G. Zhang, Y. He, Y. Feng, H. Wang, T. Zhang, W. Xie and X. Zhu, *J. Cleaner Prod.*, 2018, **199**, 62–68.
59 B. Li, M. Yu, Z. Li, C. Yu, Q. Li and H. Wang, *J. Energy Storage*, 2022, **51**, 104515.
60 L. Tian, M. Wang, L. Xiong, C. Huang, H. Guo, S. Yao, H. Zhang and X. Chen, *Electroanal. Chem.*, 2019, **839**, 264–273.
61 G. Zhang, X. Yuan, Y. He, H. Wang, W. Xie and T. Zhang, *Waste Manage.*, 2020, **115**, 113–120.